Supporting information for: Smoothing of Contact Lines in Spreading Droplets by Trisiloxane Surfactants and its Relevance for Superspreading

Rolf E. Isele-Holder,[*,†,‡] Benjamin Berkels,[‡] and Ahmed E. Ismail[*,†,‡]

Aachener Verfahrenstechnik: Molecular Simulations and Transformations, RWTH Aachen University, Schinkelstraße 2, 52062 Aachen, Germany, and AICES Graduate School, RWTH Aachen University, Schinkelstraße 2, 52062 Aachen, Germany

E-mail: isele@aices.rwth-aachen.de; aei@alum.mit.edu

This document describes further details of the setup and the analysis of the spreading simulations. In Section 1, we provide further details about the simulation setup and the computational effort. Results for the analysis of local temperatures and velocities are given in Sections 2 and Section 3.

1 Simulation Setup and Computational Effort

Information on the simulation setup is summarized in Table S1.

The simulations were run on Hydra at the RZG located at Garching in Germany. Simulations were performed on either the Sandy Bridge or Ivy Bridge Nodes available on the

[*]To whom correspondence should be addressed
[†]Aachener Verfahrenstechnik: Molecular Simulations and Transformations, RWTH Aachen University, Schinkelstraße 2, 52062 Aachen, Germany
[‡]AICES Graduate School, RWTH Aachen University, Schinkelstraße 2, 52062 Aachen, Germany

Table S1: Details on the simulation setup

simulation	n_{pol}[a]	n_{wat}[b]	$n_{\mathrm{surf,bulk}}$[c]	$n_{\mathrm{surf,int}}$[d]	A_{mol}[e] [Å^2]	radius[f] [Å]	Lx[g] [nm]	Ly[h] [nm]	Lz[i] [nm]
PP, T6	300	55569	52	800	70	135	50	8	40
PP, T3	300	78280	83	950	60	135	50	8	40
PP, T11	360	80665	50	504	115	170	60	8	50
PP, CE	300	59309	0	1078	50	135	50	8	40
PTFE, T6	310	55569	52	800	70	135	50	8	40
PEO, T6	340	55569	52	800	70	135	50	8	40

[a] number of polymer molecules; [b] number of water molecules; [c] number of surfactant molecules in the bulk; [d] number of surfactant molecules at the interfaces; [e] approximate surface area per surfactant molecule at the interface; [f] approximate initial radius of the droplets; [g,h,i] box dimensions in x, y, and z dimension;

machines. One nanosecond of simulation of the spreading droplets took in the range of 12 to 17 hours of wallclock time on 500 (Ivy Bridge) or 512 (Sandy Bridge) cores. Overall, more than 2.5 million core hours were used to perform the spreading simulations.

2 Local Temperature

The temperature T is related to the velocities of the particles by

$$T = \frac{1}{N_f k_B} \sum_{i=1}^{N} m_i \mathbf{v}_i^2, \tag{1}$$

where N_f is the number of degrees of freedom, k_B is the Boltzmann constant, the sum is over all N atoms in the system, m_i is the mass and $\mathbf{v}_i$ is the velocity vector of atom i. To compute local temperatures, the simulation box was subdivided into bins with square cross-sections in the x and z direction. Eq. 1 was evaluated separately for each bin. Because the water molecule is held rigid, it has only 6 degrees of freedom, whereas flexible molecules with 3 atoms have 9 degrees of freedom. When computing the local temperatures, 2 degrees of

freedom were assigned to each atom of the water molecules. When performing the analysis, we tried different values for the width of the bins $h \in \{1, 2, 5, 10\}$ Å. Results of the local temperatures are depicted in Figure S1.

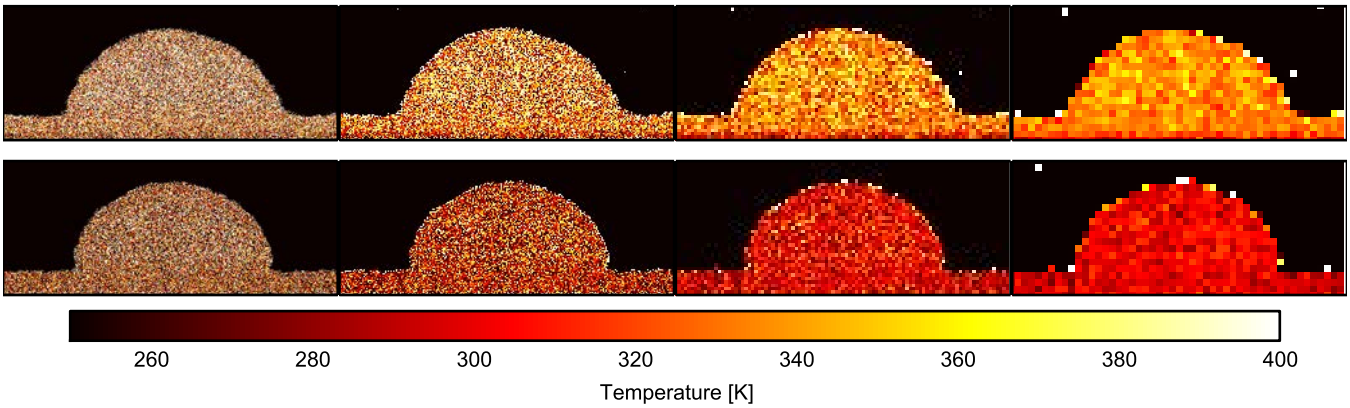

Figure S1: Local temperatures from a snapshot of the LN, PP, T6 (top) and the NH, PP, T6 (bottom) simulations. From left to right the width of the bins used to compute local temperatures increases: $h \in \{1, 2, 5, 10\}$ Å. For small bins, the data is very noisy. From the images created with larger bins it becomes obvious that the temperature is homogeneously distributed in both droplets. The major difference is that the droplet with the LN simulation has a higher average temperature for reasons discussed in the main article.

3 Velocity Field

To compute instantaneous velocities, the simulation domain was subdivided into bins with square cross-sections in the xz plane with a width of 1 Å in each direction. Similar to the local densities, the center-of-mass velocities in each bin were computed every timestep and averaged over 10 ps. The average velocities were used to create vector fields. To reduce the noise in the data, additional averages over multiple bins were taken during the post-processing of the data. The averages for multiple bins were computed by taking mass-weighted averages of the velocities of multiple bins. Results for the velocity fields are shown in Figure S2 for averaged velocities over 10 ps for a selected snapshot from the NH, PP, T6 simulation.

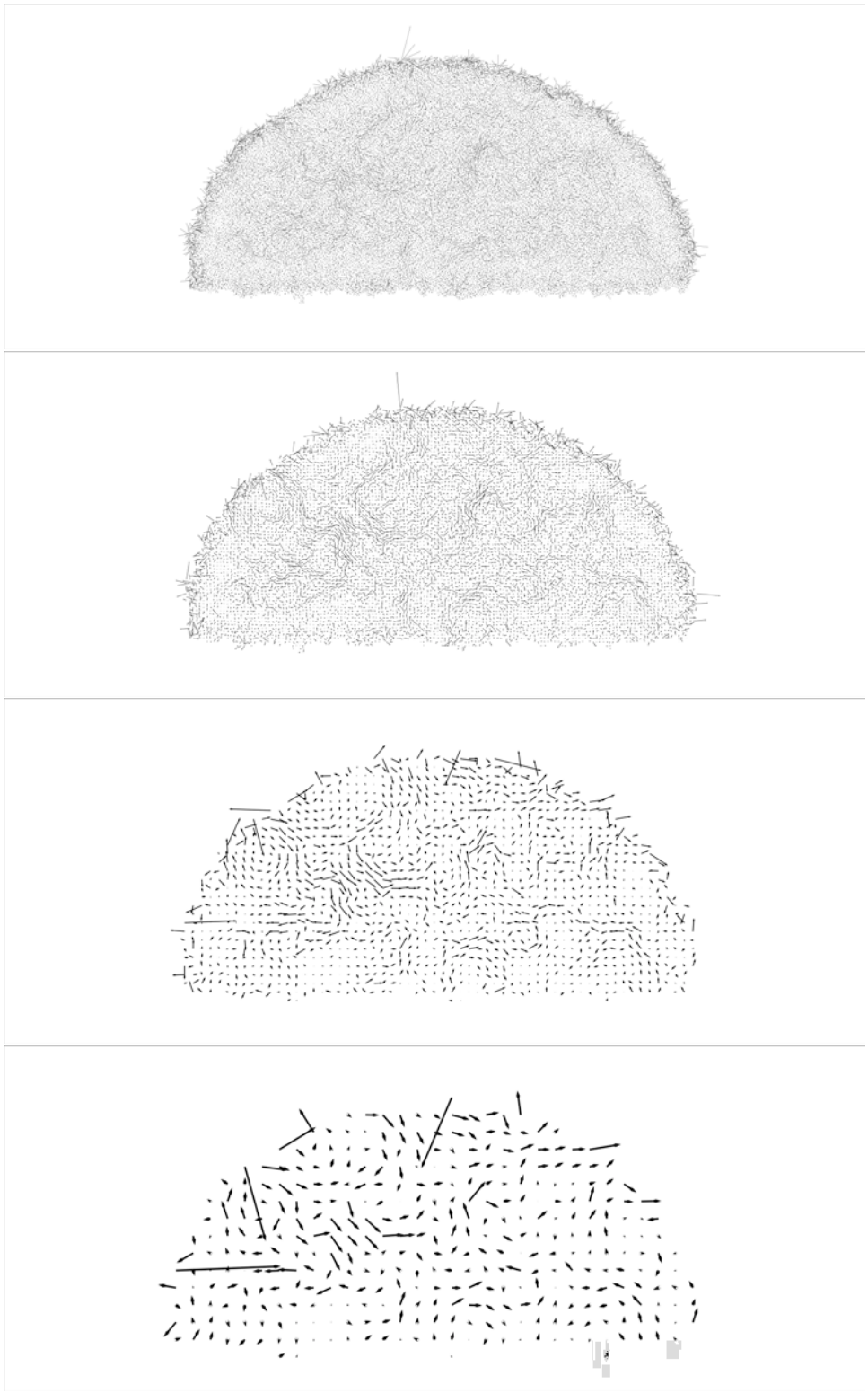

Figure S2: Velocity fields of the NH, PP, T6 simulation. From top to bottom the width of the bins used to compute the local velocity changes from $h = 1\,\text{Å}$ via $h = 2\,\text{Å}$ and $h = 5\,\text{Å}$ to $h = 10\,\text{Å}$. No meaningful flow patterns can be extracted from the data because it is too noisy.

4 Influence of the cut-off ϵ in the moment-based surface analysis

In this section, we briefly adress the impact of the cut-off ϵ used for the moment-based surface analysis. First, to highlight features of the method and the chosen cut-off, we present an example for a very simple geometry. Based on the key features presented there, we justify the specific choice of ϵ for the analysis described in the main article. Afterwards, we present results for the droplet analysis when using smaller or larger cutoffs compared to the choice in the main text.

The geometry we use in our example are two rounded edges with different curvatures as depicted in Figure S3a. The radius at the corner of the left shape is 100 in arbitrary distance units, whereas the radius of the right shape is 250. Both shapes can be thought of being infinitely extended to the bottom and the left; Figure S3a thus only shows a small fraction of the shapes. Figures S3b to S3h show the edge of the shape color coded with the value for the image classifier obtained when using different values for ϵ. The width of the black bar in each image corresponds to the value of ϵ. The color code is the same for each fixed value of ϵ but varies for different choices of ϵ. In each image, the maximum value of the image classifier corresponds to dark red (obtained at the apex of the sharper corner), whereas the minimum value is deep blue and is obtained for all points on the surface with a distance of more then ϵ from the rounded edge. In addition to the plots, Table S2 summarizes characteristic results of the analysis. In this table, C_{min} is the minimum value of the surface classifier that is obtained far away from the corner, and $C_{\mathrm{max},100}$ and $C_{\mathrm{max},250}$ are the maximum values of the classifier obtained for the shapes with a radius of 100 and 250, respectively.

For the selected example, it is clear that there is a difference in the two shapes. In the following, we will show that the choice of ϵ has an impact on how well the shapes can be distinguished via the surface classifier, but that the choice of ϵ does not lead to the identification of spurious artefacts (e.g., that the corner with the larger radius is identified

as being sharper).

A quick inspection of the colors on the surface immediately reveals that the darkest red in each subfigure is found at the apex of the corner of the left shape, meaning that the left shape is always identified as the one with the sharper corner. The analysis does thus not produce any artefacts. What is influenced by the choice of ϵ, however, is how well the two shapes can be distinguished. As can be seen from the color of the shapes, the right corner achieves comparable values for the image classifier when using either a very small or a very large ϵ (cf. Figure S3b and Figure S3h). In contrast, for intermediate values of ϵ that are comparable to the size of the radii, as in Figures S3d and S3e, there is a strong difference between the colors of the left and the right shape, meaning that the classifier provides a better differentiation of the shapes.

This effect can be seen more quantitatively from Table S2. The value of $C_{\min}$ is rather insensitive to the choice of ϵ, whereas both $C_{\max,100}$ and $C_{\max,250}$ grow with increasing ϵ. For very small ϵ, $C_{\max,100}$ and $C_{\max,250}$ are only slightly larger than $C_{\min}$, meaning that the curved region can here hardly be distinguished from the flat region away from the corner based on the image classifier. At the extreme of very large values of ϵ, $C_{\min}$ is strongly different from $C_{\max,100}$ and $C_{\max,250}$, but $C_{\max,100}$ and $C_{\max,250}$ are not very distinct. An easy differentiation of all three values, $C_{\min}$, $C_{\max,100}$, and $C_{\max,250}$ is only possible for intermediate values of ϵ that are of similar size as the differences in the shapes that need to be characterized. In particular, as can be seen from the last column of Table S2, the differentiation of $C_{\max,100}$ and $C_{\max,250}$ works best for $\epsilon = 250$, which matches the radius of the corner of the right-hand shape.

The observations described in the last paragraph can be best understood when considering that ϵ determines the scale on which a shape is examined. A small ϵ corresponds to examining the shape only in the close vicinity of a given point, resulting in that the object is classified as flat, just like the earth appears flat to humans that are close to the surface of the earth compared to its curvature. For a very large ϵ, the object is characterized on the

large scale in which both corners look almost spiky. The difference between the shapes can only be identified when examining the appropriate scale.

The findings from this simple example can be transferred directly to the analysis of the droplet shapes. A bad choice of ϵ does not artificially identify non-existant features, while significant differences in shape can only be well identified for values of ϵ that are comparable to the characteristic size of the examined shape. As shown in the previous example, differentiation of the shapes worked best when ϵ is similar to the radius of the smoother corner. We therefore chose $\epsilon = 20\,\text{Å}$ for our analysis, because this approximates the radius of the corner for the PP, T6 simulation, as can be seen from Figure S4.

For the sake of completeness, we show results obtained when using a larger or a smaller ϵ in Figure S5. Results obtained from the PP, T6 and the PP, CE simulations are best separated for the middle image with $\epsilon = 20\,\text{Å}$. The separation is less obvious for both smaller and larger ϵ. As can be seen from the simple example above, however, this does not show that there is no difference between the shapes; it only shows that the larger or smaller ϵ are not capable of detecting the existing differences.

To conclude, we have selected ϵ in the moment-based surface analysis so that existing differences between the shapes are emphasized, while the classifier did not lead to "false positives" for any of the tested values of ϵ.

Table S2: Characteristic values of the surface classifier for the simple example.

ϵ	C_{min}	$C_{\text{max,100}}$	$C_{\text{max,250}}$	$C_{\text{max,100}} - C_{\text{min}}$	$C_{\text{max,250}} - C_{\text{min}}$	$C_{\text{max,100}} - C_{\text{max,250}}$
25	0.450153	0.469017	0.468079	0.018864	0.017926	0.000938
50	0.446272	0.465686	0.457028	0.019414	0.010756	0.008658
100	0.444741	0.494536	0.456171	0.049795	0.01143	0.038365
250	0.444587	0.549059	0.491526	0.104472	0.046939	0.057533
500	0.444493	0.567506	0.537757	0.123013	0.093264	0.029749
625	0.444491	0.570976	0.547782	0.126485	0.103291	0.023194
1250	0.444607	0.578261	0.566896	0.133654	0.122289	0.011365

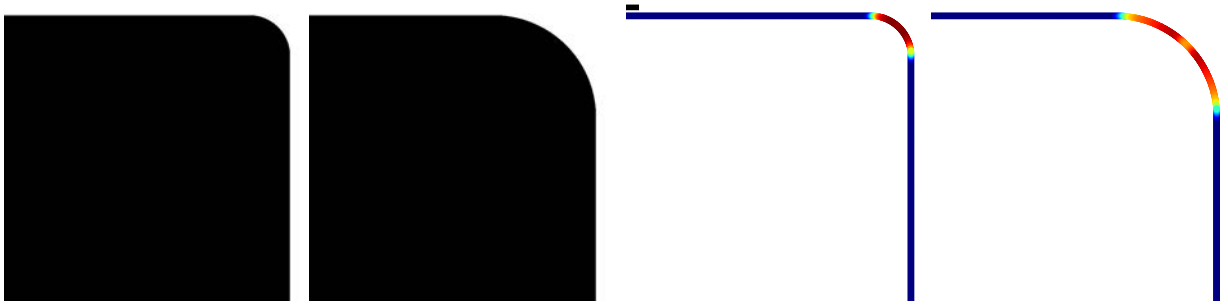

(a) Shapes

(b) $\epsilon = 25$

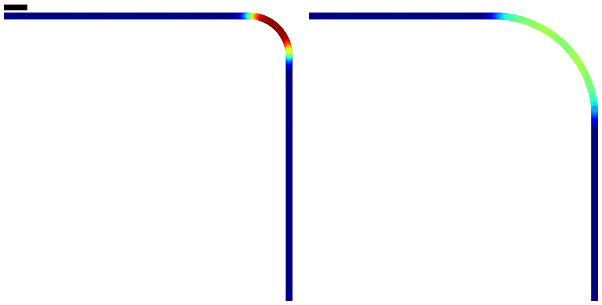

(c) $\epsilon = 50$

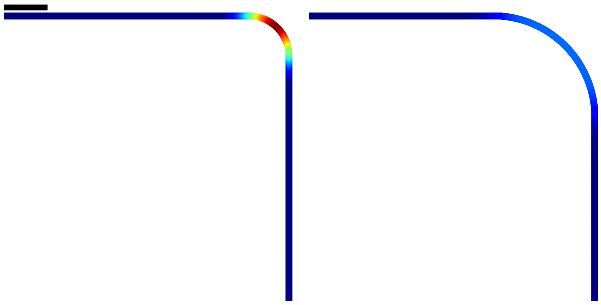

(d) $\epsilon = 100$

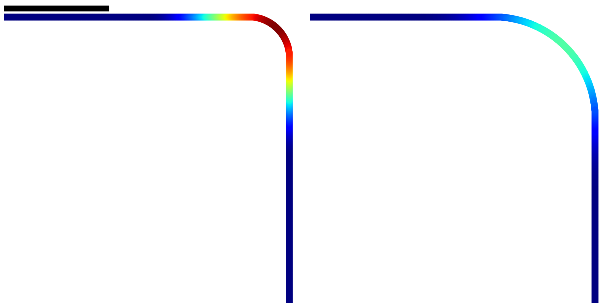

(e) $\epsilon = 250$

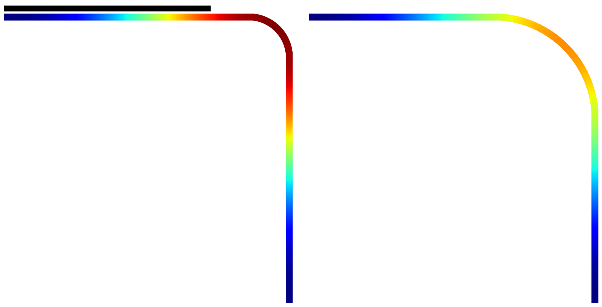

(f) $\epsilon = 500$

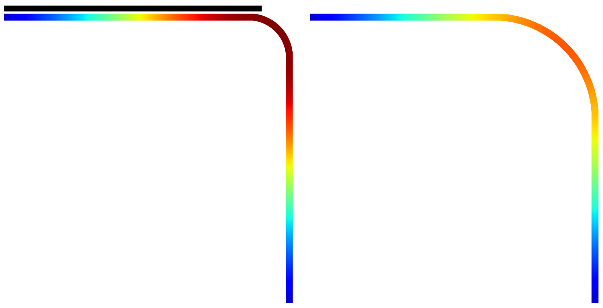

(g) $\epsilon = 625$

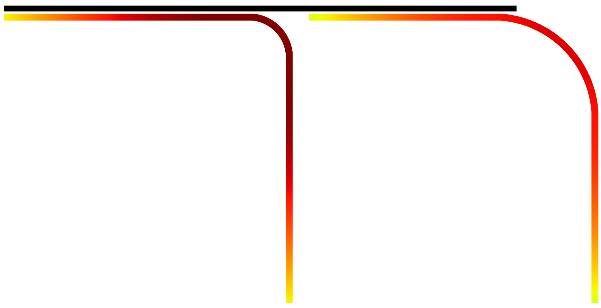

(h) $\epsilon = 1250$

Figure S3: Effect of the moment-based surface classifier for a simple geometry. Upper left: examined shapes; other images: surface of the shapes color coded with the surface classifier for different ϵ as specified in the subheadings.

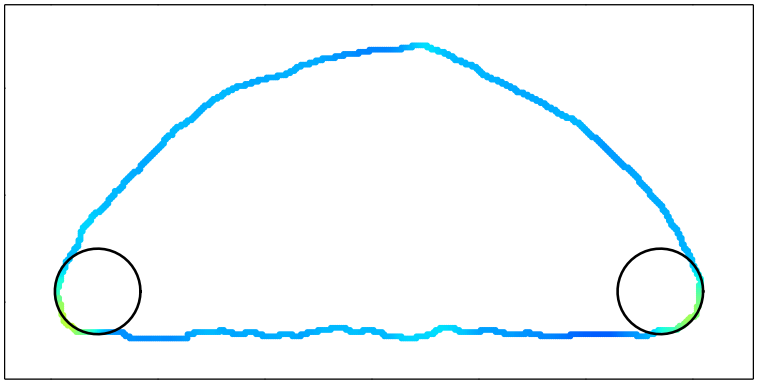

Figure S4: Surface of the droplet from the PP, T6 simulation color coded with the surface classifier. The black circles in the lower left and lower right corner have a radius of 20 Å, which is the value of ϵ used in the analysis in the main text.

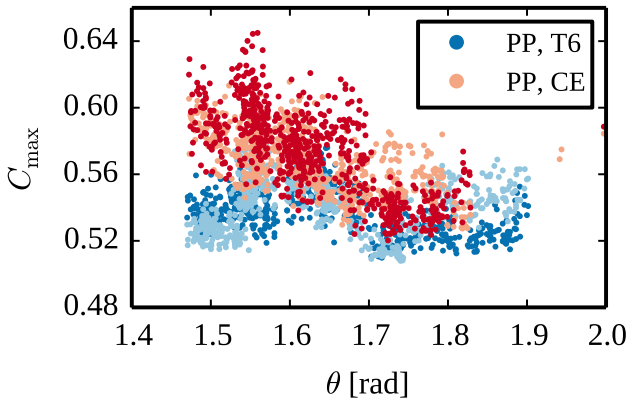

(a) $\epsilon = 10\,\text{Å}$

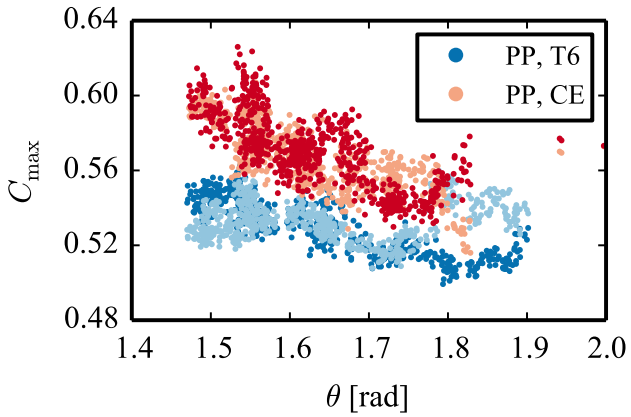

(b) $\epsilon = 20\,\text{Å}$

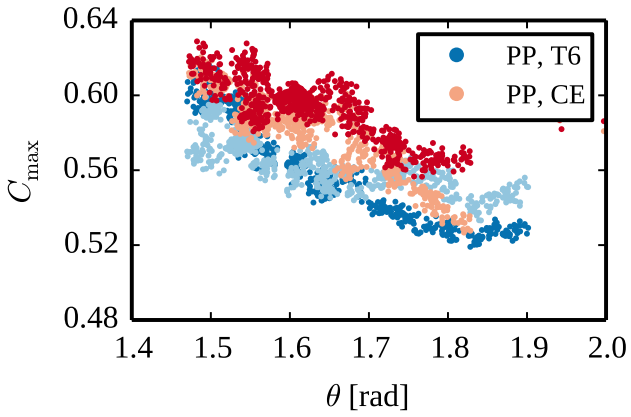

(c) $\epsilon = 40\,\text{Å}$

Figure S5: Maximum surface classifier over the contact angle for the PP, T6 simulation for different ϵ as specified in the subcaptions. The red and blue points are best separated for $\epsilon = 20\,\text{Å}$.